



# Realizing fast plating/stripping of high-performance Zn metal anode with a low Zn loading

Zhuo LI<sup>1</sup>, Tamene Tadesse BEYENE<sup>2</sup>, Kai ZHU<sup>1,\*</sup>, and Dianxue CAO<sup>1</sup>

<sup>1</sup>Key Laboratory of Superlight Material and Surface Technology of Ministry of Education College of Material Science and Chemical Engineering, Harbin Engineering University 145 Nantong Street, Harbin 150001, P. R. China

<sup>2</sup>Department of Chemistry, College of Natural Sciences, Jimma University, P.O.Box 378, Jimma-Ethiopia

\*Corresponding author e-mail: kzhu@hrbeu.edu.cn

Received date:  
25 March 2024

Revised date  
10 April 2024

Accepted date:  
17 April 2024

## Keywords:

Aqueous battery;  
Energy storage;  
Flexible interface;  
3D current collector;  
Zn metal anode

## Abstract

Zn metal batteries and capacitors (ZMBs/ZMCs) are gaining significant attention due to their low cost, high safety, and high theoretical capacity. However, the low utilization of Zn metal decreases the coulombic efficiency. Here, we present a novel approach to enhance the conductivity of host materials by utilizing a 3D conductive structural network of copper mesh. The 3D copper mesh serves as a high-conductive matrix and additionally coating it with Zn serves as a Zn source. Finally, a flexible reduced graphene oxide (rGO) was deposited on the Zn-coated copper mesh as an anode protective layer. The conductive copper mesh renders a fast plating/stripping of Zn and enables more contact of Zn with the electrolyte. The flexible rGO film deposited on Zn-coated copper mesh alleviates the local charge accumulation and inhibits corrosion. As a result, the Zn-coated copper mesh anode modified with rGO (RCZ) exhibited a longer lifespan of 200 h than the Zn-coated planar copper foil anode which cycled only for 30 h. The RCZ||AC full capacitor obtained high capacity retention of 97.9% after 9000 times cycling. The RCZ anode integrates the merits of 3D structure matrix and rGO realizing a dual-functionalized Zn metal anode. The conductive matrix strategy sheds light on other metal batteries.

## 1. Introduction

Zn metal batteries/Zn metal capacitors (ZMBs/ZMCs) possessing low cost, relative safety, low redox potential, and environmental benign have gathered vast interest in recent years [1,2]. As a result of their feasible manufacturing cost and safety merit, ZMBs/ZMCs are suitable candidates for grid-scale energy storage systems [3,4]. However, the notorious hydrogen evolution reaction (HER) and other parasitic reactions hinder the reversibility of the Zn metal anode and decrease its utilization as a negative electrode [5]. Furthermore, the uncontrolled formation and dendrite growth are likely to be the underlying cause of inner short circuits [6]. Due to the disordered charge distribution on the Zn anode, the deposition kinetics on a Zn metal anode are significantly altered [7]. This will accelerate dendrite growth or formation of dead Zn by stimulating the tip-growth of Zn [8]. Therefore, addressing the problem with the anode in aqueous ZMBs is of utmost importance.

As of now, three types of strategies have been employed to mitigate these issues: electrolyte additives, membrane modifications, surface engineering, and matrix modification [9,10]. The addition of the proper amount of additives can alter the structure of the solvation shell surrounding hydrous Zn-ion, thereby facilitating the desolvation process. Recently, Zhang *et al.* highlighted the significance of incorporating an adequate level of iodide ion into the conventional zinc sulfate (ZSO) electrolyte to inhibit dendrite growth and dead Zn formation

in the ZMBs/ZMCs cell [11]. However, excessive additives reduced electrolyte conductivity and raised overpotentials. The surface engineering is easy and facile approach to execute on Zn surface and mitigate dendrite growth on the negative electrode during cycling [12]. The use of organic and inorganic materials is extensively investigated in ZMBs/ZMCs to create a protective layer that serves as an artificial solid electrolyte interface (SEI) [13] Mao *et al.* employed guar-gum on Zn surface obtaining a prolonged lifespan of Zn metal anode [14]. The guar-gum is a kind of natural organic material containing plenty of hydrous functional groups. Polyacrylonitrile (PAN) [15], polyacrylamide (PAM) [16] were also investigated as the modifiers Zn metal anode. Various forms of inorganic artificial SEI including metal materials (pure metal and alloys [17]), semiconductors (transition metal oxides [18], sulfides [19]), functional 2D carbon materials (rGO [20], MXene [21]) were investigated in aqueous battery research. Metallic protective layers are typically stable due to their superior mechanical strength, which helps resist corrosion in aqueous environments and volume expansion during the charging and discharging process. In-situ fabrication of a Tin metal layer on a Zn metal surface has successfully achieved homogeneous deposition and corrosion inhibition [22]. However, the use of Zn beneath the layer is inadequate due to the integration of the current collector and anode function. Owing to the strong effect of metal, the kinetic of Zn during cycling can be confined. From this perspective, a 3D structure can provide

more contact with the electrolyte of Zn-ions which is beneficial for the charge transfer. The common metal anode such as lithium and zinc metal, is much more than the capacity that cathode provides which lower the mass capacity of overall cell. In this condition, the efficient utilization of zinc metal is full of significance. The deposited Zn on copper mesh minimizes the loading of metal and separate the function of anode and current collector on Zn. The current collector of copper mesh express a high efficiency of electron transfer inhibiting the side-reactions.

Mu *et al.* utilized graphene to obtain a 3D anode realizing an ultra-long cycling lifespan of Zn metal anode [23]. Liu *et al.*, on the other hand, utilized a 2-methylimidazole zinc salt (ZIF-8) and graphene scaffold to achieve a uniform deposition of the Li metal anode [24]. The 3D ZnF<sub>2</sub> matrix was also chosen as an anode matrix and has achieved an extremely long lifespan for Zn metal anodes [25]. The 3D structure design can significantly enhance the electrochemical performance of the Zn metal anode. Furthermore, the physical and chemical characteristics of rGO are well-suited for enhancing the electrochemical performance of the Zn metal anode [26]. The flexibility of rGO enables it to resist changes in structure and morphology while increasing conductivity to facilitate charge redistribution. Due to these advantages, rGO can also be incorporated into ZMBs/ZMCs.

Here, we present a 3D high-conductive framework featuring a self-assembling rGO film to achieve a highly reversible and electrochemical performance of Zn metal anode. The 3D copper mesh acts as the high-conductive matrix, with the Zn coating of the copper mesh serving as the zinc source (referred to as CZ). Compared to those

2D conductive materials such as graphene, MXene, the commercial 3D copper mesh expresses a high electronic transfer efficiency and fast 3D diffusion with a low cost. With the complex and toxic preparation process of graphene, MXene, the 3D copper mesh was environmental friendly which is consistent with the inherent demand of energy storage. Subsequently, the rGO is applied onto the Zn-coated copper mesh as a protective layer (referred to as RCZ). The conductive copper mesh facilitates a quicker deposition/stripping of Zn and enhances the contact of Zn with the electrolyte. The flexible rGO film-coated CZ mitigates local charge accumulation and inhibits corrosion. In a symmetrical cell with the 3D RCZ anode, a lifespan of 200 h was achieved, surpassing the 30 h lifespan of a flat Zn plated on copper foil (FCZ) anode, indicating improved anode reversibility and corrosion inhibition. The cycling performance of full capacitors was also evaluated in a coin cell paired with active carbon (AC), revealing a high capacity retention of 97.9% after 9000 cycles. The RCZ anode combines the advantages of a 3D structural matrix and rGO to create a dual-functionalized Zn metal anode. The conductive matrix approach mitigates charge accumulation, shedding light on its applicability to other metal batteries.

## 2. Results and discussion

The preparation of RCZ can be understood as two main parts: the preparation of Zn-plated copper mesh (CZ) and the rGO coating (self-assembling) (Figure 1(a)). The operational details can be referred to the Experimental section in Supplementary information. Firstly, the Zn

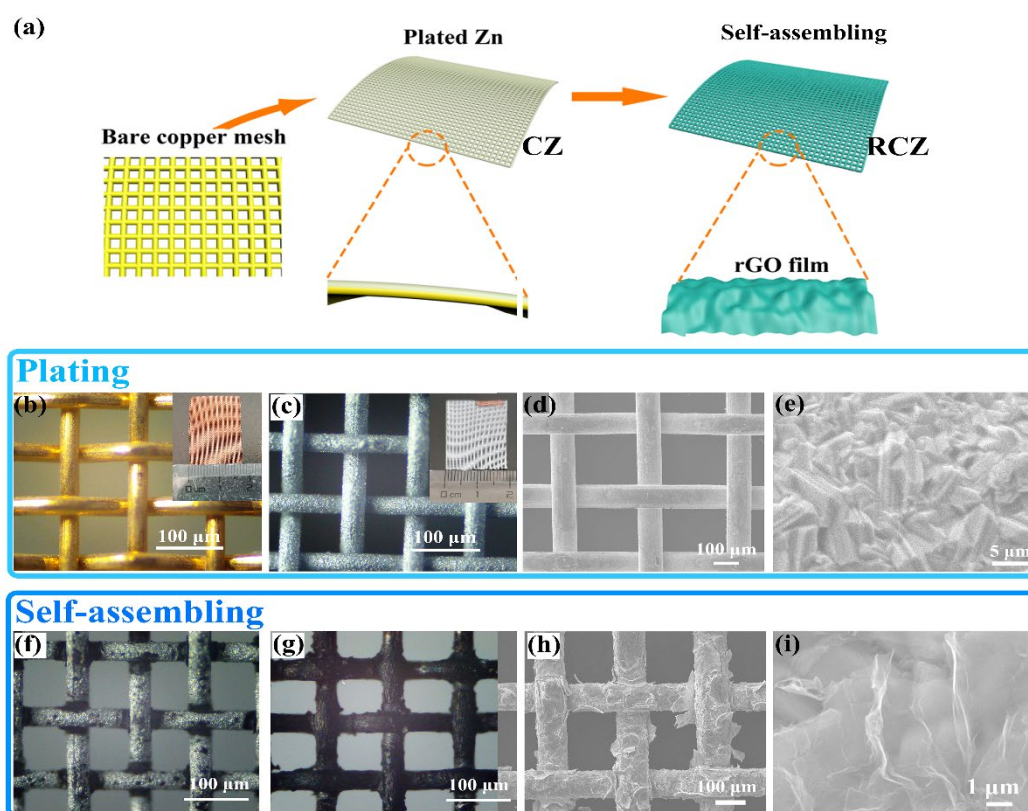


**Figure 1.** The preparation of RCZ. (a) The scheme of modification process, The digital images of original (b), and Zn plated copper mesh (c), (d-e) The SEM images of Zn plated copper mesh, The digital images of Zn plated copper mesh immersed in GO solution for 1 min (f), and 3 min (g), and (h-i) The SEM images of RCZ.

source was fabricated by electroplating,  $80 \text{ mA}\cdot\text{cm}^{-2}$  is the optimal current density without copper mesh exposure and Zn agglomerations. With 15 min duration, the Zn was homogeneously plated on copper mesh through the optical microscope (Figure 1(b-c)). To further analyze the crystal texture of plated Zn, the scanning electron microscope (SEM) was employed. As shown in Figure 1(d), the Zn-plated copper mesh was smooth and uniform, the magnified images show a proper crystal particle of  $5 \mu\text{m}$  (Figure 1(e)). Secondly, the rGO protective layer was self-assembled on Zn-plated copper mesh. Based on the concentration of rGO of  $1 \text{ mg}\cdot\text{mL}^{-1}$ , the rGO self-assembly grew on the Zn surface. With different duration periods in rGO solution, the wrapping status of Zn changes much. When CZ was immersed for 1 min, it was not enough for rGO to react with Zn metal leaving a large exposure on the Zn surface (Figure 1(f)). With the time extended to 2 min, the Zn was coated perfectly as shown in Figure 1(g). However, the rGO gradually got into cracks when continued to extend the duration. In this condition, the Zn will be directly exposed to aqueous surroundings without protection (Figure 1(h)). The SEM image (Figure 1(i)) shows the thin rGO film with fine wrinkles on the Zn surface. The perfect wrapping is beneficial to corrosion inhibition. Additionally, the outstanding conductivity of rGO with comprehensive coating effectively alleviates the charge accumulation.

To further analyze the Zn texture on copper mesh and rGO, X-ray diffraction (XRD) and Fourier transform infrared (FTIR) tests were conducted. The XRD spectrum and PDF identification card are depicted in Figure 2(a). The diffraction peaks at  $43.32^\circ$ ,  $56.45^\circ$ , and  $74.12^\circ$  correspond to the (111), (200), and (220) crystal facets of Zn metal, respectively. The peaks at  $36.29^\circ$ ,  $38.99^\circ$ ,  $43.22^\circ$ ,  $54.32^\circ$ , and  $70.07^\circ$  correspond to the (002), (100), (101), (102), and (103) crystal facets of the copper mesh, respectively. Due to the close diffraction angles to the (111) crystal plane of copper and the (101) crystal plane of zinc, they merge into a single strong peak around  $43.3^\circ$ . This suggests successful deposition of the zinc layer on the 3D copper network. The wide peak between  $20^\circ$  and  $30^\circ$  ( $\sim 25^\circ$ ) likely represents reduced graphene oxide. FTIR analysis of dried GO and rGO on the RCZ electrode (Figure 2(b)) further confirms the successful self-assembly of rGO. The reduction in the peak at  $1600/\text{cm}$  indicates a decrease in C=O double bonds, suggesting a reduction in oxygen-containing functional groups during the graphene oxide reduction process. This reduction results in the restoration of more conjugate structures, enhancing electrical conductivity. Enhanced electrical conductivity enables rapid electron conduction and decreases the overpotential of zinc during deposition and dissolution.

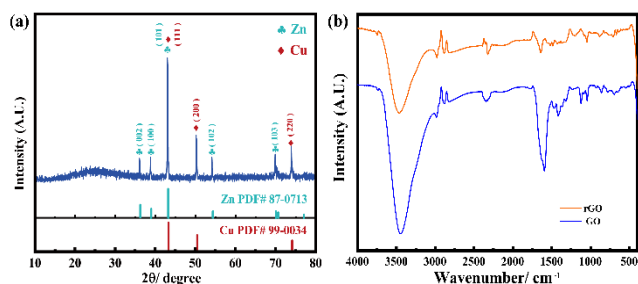


**Figure 2.** (a) The XRD spectrum of plated Zn, and (b) The FTIR spectrum of rGO and GO.

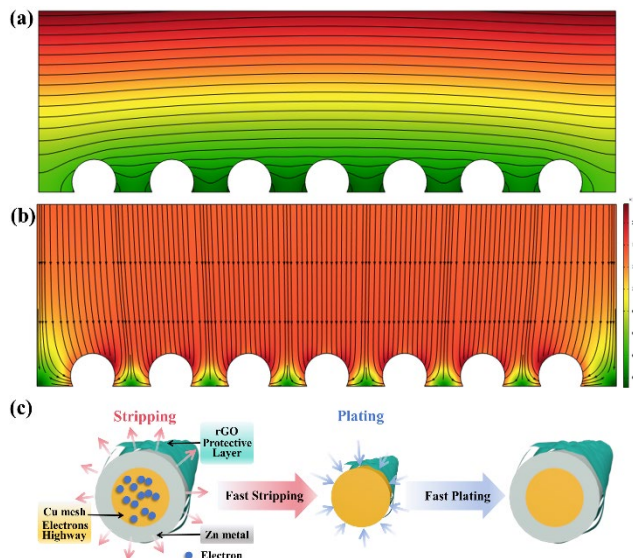


**Figure 3.** The rapid charge transfer mechanism on RCZ. (a) The simulation of voltage distribution, (b) The cross image of current density distribution, and (c) The scheme of plating/stripping process of Zn on RCZ.

To analyze the current density distribution, and exchange of RCZ during the plating/stripping process, a second current density distribution was simulated. The potential contour lines reveal a lower level around the copper mesh, indicating a swift reaction in that vicinity (Figure 3(a)). The distribution of current density highlights the active Zn plating/stripping area, with rapid reactions concentrated near the copper mesh. This suggests that the copper mesh offers superior conductivity compared to other forms (Figure 3(b)). The mechanism, illustrated in the diagram (Figure 3(c)), shows how copper acts as an electron highway, facilitating the rapid flow of electrons. Compared to the common 2D planar Zn on Cu, the electronic highway on 3D copper mesh expressed a high efficient utilization of Zn which inhibited the HER and other parasitic reactions. As a result, the limited Zn can avoid unnecessary consumption leading to a prolonged lifespan of symmetrical cells. Consequently, the Zn metal surrounding the copper mesh undergoes fast stripping. Moreover, rGO was utilized as a protective layer to prevent Zn corrosion.

Galvanostatic charge-discharge tests were conducted in symmetrical cells to determine the plating and stripping properties of the RCZ anode. The density used was  $0.25 \text{ mA}\cdot\text{h}\cdot\text{cm}^{-2}$ , and the current density was  $0.5 \text{ mA}\cdot\text{cm}^{-2}$  (Figure 4(a)). At the start of the second cycle, the overpotential of RCZ was  $20.4 \text{ mV}$ , and for CZ, it was  $24.8 \text{ mV}$ . The results showed that compared to CZ, reduced graphene oxide did not increase the overpotential of the reaction but instead decreased it slightly. This indicates that most of the oxygen-containing functional groups on the surface of rGO were reduced, and the rGO had excellent electrical conductivity due to its abundance of free electrons.

After 29 h of cycling, the CZ||CZ symmetrical cell showed a significant decline, and the overpotential surged, indicating that corrosion or dendrite formation was hindering the cycle on the electrode surface. On the other hand, the RCZ anodes achieved a stable cycling of 228 h, and the overpotential was only  $34.7 \text{ mV}$  at 228 h. The electrochemical impedance spectroscopy (EIS) tests also indicated a fast charge transfer process on RCZ (Figure 4(b)).

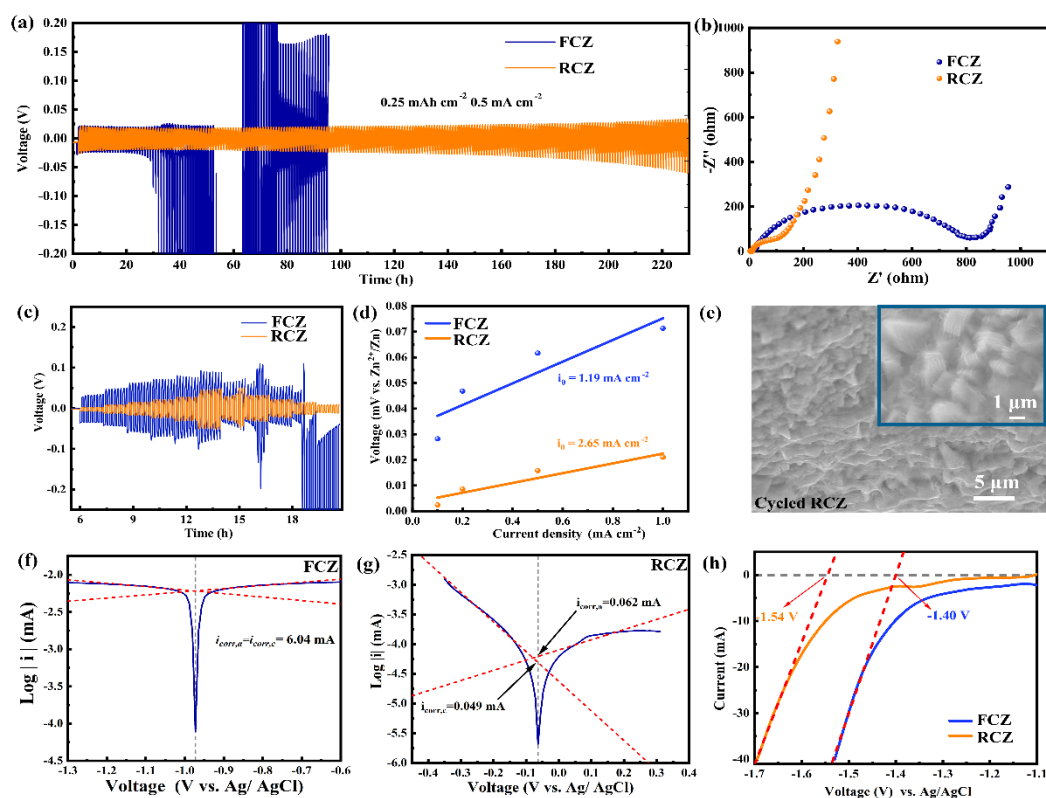


**Figure 4.** The electrochemical performance of RCZ anode. (a) The galvanostatic charge-discharge curves of symmetrical cells, (b) The EIS plots of symmetrical cells, (c) The rate performance of symmetrical cells, (d) The fitting curves of overpotential and current densities, (e) The SEM images of cycled RCZ anodes, The tafel curves of bare Zn (f) and RCZ (g), and (h) LSV curves of bare Zn and RCZ.

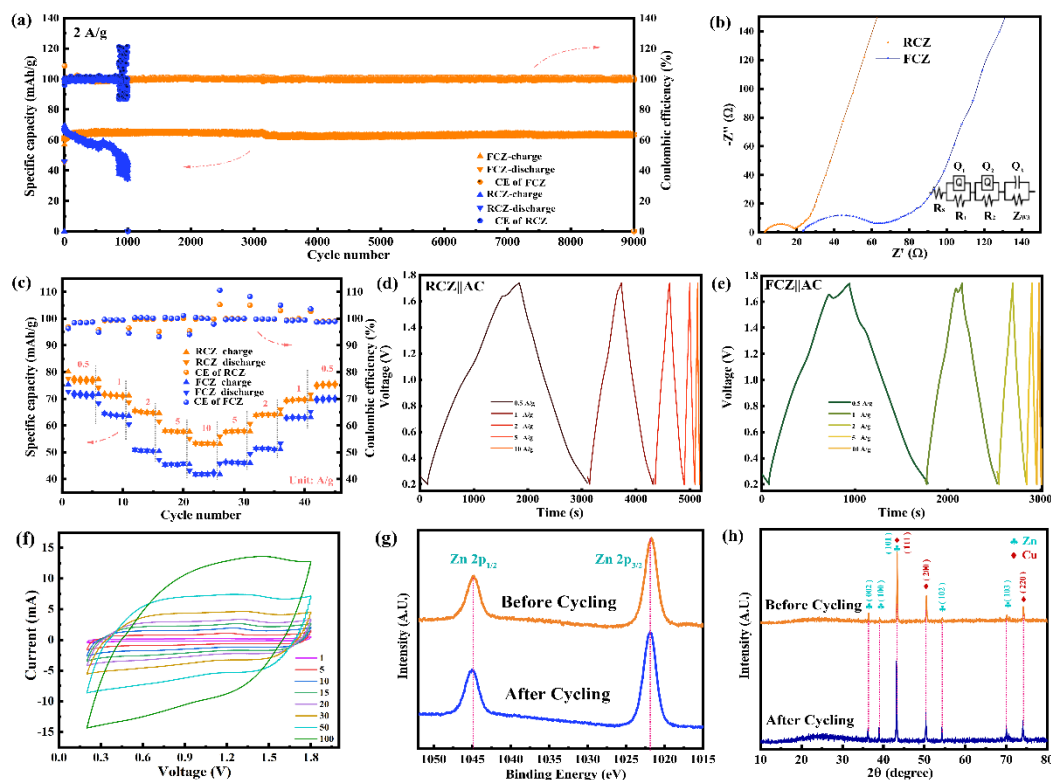


**Figure 5.** The electrochemical performance in full capacitors. (a) The galvanostatic charge-discharge plots of capacitors, (b) The EIS plots of fresh full capacitors, (c) The rate performance of capacitors, (d)-(e) The charge-discharge profiles in rate tests, (f) The CV curves of RCZ ||AC, (g) The XPS high-resolution curves of fresh and cycled RCZ anodes, and (h) The XRD spectrum of fresh and cycled RCZ anodes.

The rate performance of the RCZ anode was also evaluated in symmetrical cells. The current densities applied to the electrode were 0.5, 1, 2, 5, 10, 15, 10, 5, 2, 1, 0.5 mA·cm<sup>-2</sup>. The initial overpotential of RCZ was only 2.1 mV, while that of CZ was 31 mV (Figure 4(c)). At the maximum current density, the overpotential of RCZ was only 44.6 mV, while that of CZ had increased to 92 mV. When the current density returned to 5 mA·cm<sup>-2</sup>, the CZ showed abnormal fluctuations, which may be caused by large pieces of surface zinc falling off after experiencing a large current cycle. When the current density returned to 1 mA·cm<sup>-2</sup>, the CZ symmetric cells failed which may be attributed to the dendrites growth. In contrast, the overpotential of RCZ was 8.6 V at 1 mA·cm<sup>-2</sup>, indicating that the modification improved the rate performance by facilitating charge transfer.

The current density-overpotential lines were linearly fitted, and the exchange current densities of the chemical reaction on the electrode surface were calculated by the slope of linear fitting lines (Figure 4(d)). The exchange current density of RCZ was 2.65 mA·cm<sup>-2</sup>, which was higher than that of pure zinc electrodes (1.19 mA·cm<sup>-2</sup>), indicating a faster reaction on RCZ than on CZ. The morphology of cycled RCZ was analyzed by SEM. The SEM images suggested an intact rGO film on the Zn metal, and the Zn metal under the film was smooth.

To explore the corrosion resistance of the electrodes, the Tafel tests were executed. The corrosion current density of CZ is 6.04 mA·cm<sup>-2</sup>, and that of RCZ is 0.049 mA·cm<sup>-2</sup>. The result shows that the modified electrode has excellent corrosion resistance compared with CZ (Figure 4(f-g)). To investigate the hydrogen evolution inhibition performance of the modified electrode, the linear sweep voltammetry (LSV) tests were performed in the three-electrode system (Figure 4(h)). The HER potential is -1.54V than that of CZ (-1.40V). These results indicate that the modified electrode can inhibit the hydrogen evolution reaction. Zinc deposition and hydrogen deposition are competitive reactions, but the HER is thermodynamic preference and deposition is kinetic preference, so the high conductivity of RCZ is beneficial to Zn deposition, thus inhibiting the hydrogen evolution reaction [27].

To assess the RCZ performance in full capacitors, they were made with an active carbon (AC) cathode using a 2M ZnSO<sub>4</sub> electrolyte. The capacitor maintained a consistent capacity of 63.92 mAh·g<sup>-1</sup> over 9,000 cycles with a capacity retention of 97.9% at 2 A·g<sup>-1</sup>. Initially, the Zn||AC capacitor had a capacity of 69.45 mAh·g<sup>-1</sup>, slightly higher than RCZ||AC. However, the discharge capacity dropped to 55.38 mAh·g<sup>-1</sup> by the 561<sup>st</sup> cycle, with a retention of 79.74%. This decline may be due to side reactions forming insulating by-products on the surface, hindering zinc ion electron flow. The study indicates that RCZ's good electrical conductivity and increased contact area with the electrolyte lead to uniform zinc ion plating, suppressing hydrogen evolution (Figure 5(a)). EIS confirmed RCZ's fast charge transfer in full capacitors (Figure 5(b)). Rate performance tests at different current densities revealed RCZ||AC discharged at 76.54 mAh·g<sup>-1</sup> at 0.5 A·g<sup>-1</sup> and 65.47 mAh·g<sup>-1</sup> at 2 mA·g<sup>-1</sup>, with a 14.46% decrease. Conversely, Zn||AC saw a significant capacity drop at 2 A·g<sup>-1</sup>, with a 28.65% reduction. RCZ anodes demonstrated stable deposition and stripping at varying current densities, maintaining stability even at high rates. After cycling, RCZ||AC retained 98.07% capacity, compared to Zn||AC's 97.82% (Figure 5(c)). Charge-discharge profiles at different densities are shown in Figures 5(d-e). RCZ||AC exhibited IR drops of 56.0 mV and 90.4 mV at 5 A·g<sup>-1</sup> and 10 A·g<sup>-1</sup>,

respectively. In contrast, Zn||AC showed higher IR drops at 5 A·g<sup>-1</sup> (113.8 mV) and 10 A·g<sup>-1</sup> (172.1 mV), indicating lower electrical conductivity in the zinc electrode compared to RCZ.

The RCZ||AC capacitor underwent a cyclic voltammetry (CV) test, with the resulting CV curves depicted in Figure 5(f). The cyclic voltammetry images present typical capacitor rectangles. Additionally, the X-ray photoelectron spectroscopy (XPS) analysis of both fresh and cycled RCZ anodes that were peeled off rGO showed little shift, indicating inhibited corrosion, as presented in Figure 5(g). The XRD spectrum of cycled Zn anodes showed the signal of rGO, suggesting its stable presence after cycling. The absence of any significant by-product peaks indicates that corrosion is suppressed, as shown in Figure 5(h).

### 3. Conclusions

We have proposed a strategy to enhance the conductivity of host materials with a 3D structure conductive network. The 3D copper mesh acts as a high-conductive matrix, on which Zn is deposited to serve as the zinc source. A protective layer of rGO is then fabricated on top of the Zn-coated copper mesh. The conductive copper mesh enables fast deposition/stripping of Zn and enhances contact of Zn with the electrolyte. The flexible rGO film-coated CZ helps prevent local charge accumulation and corrosion. The RCZ anode has a longer lifespan of 200 hours compared to a flat Zn plated on a copper foil anode of 30 hours. The RCZ||AC full capacitor has a high capacity retention of 97.9% after 9000 times cycling. The RCZ anode integrates the merits of the 3D structure matrix and rGO, resulting in a dual-functionalized Zn metal anode. The conductive matrix strategy has the potential to improve other metal batteries.

### Acknowledgements

This work was supported by Hong Kong Scholars Programs (Grant No. XJ2019024) Heilongjiang Postdoctoral Fund, China Postdoctoral Science Foundation (2019T120254, 2018M630340), the Key Laboratory of Superlight Materials and Surface Technology, Ministry of Education, the Fundamental Research Funds for the Central University of China (3072022JC0305).

### References

1. C. Li, A. Shyamsunder, A. G. Hoane, D. M. Long, C. Y. Kwok, P. G. Kotula, K. R. Zavadil, A. A. Gewirth, and L. F. Nazar, "Highly reversible Zn anode with a practical areal capacity enabled by a sustainable electrolyte and superacid interfacial chemistry," *Joule*, vol. 6, pp. 1103-1120, 2022.
2. S. D. Pu, B. K. Hu, Z. X. Li, Y. Yuan, C. Gong, Z. Y. Ning, C. Chau, S. X. Yang, S. M. Zhang, L. Q. Pi, Y. T. Tang, J. L. Yue, T. J. Marrow, X. W. Gao, P. G. Bruce, and A. W. Robertson, "Decoupling, quantifying, and restoring aging-induced Zn-anode losses in rechargeable aqueous zinc batteries," *Joule*, vol. 7, pp. 366-379, 2023.
3. M. L. Wu, Y. Zhang, L. Xu, C. P. Yang, M. Hong, M. J. Cui, B. C. Clifford, S. M. He, S. S. Jing, Y. Yao, and L. B. Hu,

- "A sustainable chitosan-zinc electrolyte for high-rate zinc-metal batteries," *Matter*, vol. 5, pp. 3402-3416, 2022.
4. Y. X. Zeng, D. Y. Luan, and X. W. Lou, "Recent advances in electrode engineering strategies for aqueous Zn-based batteries," *Chem*, vol. 9, pp. 1118-1146, 2023.
  5. B. Sambandam, V. Mathew, S. Kim, S. Lee, S. Kim, J. Y. Hwang, H. J. Fan, and J. Kim, "An analysis of the electrochemical mechanism of manganese oxides in aqueous zinc batteries," *Chem*, vol. 8, pp. 924-946, 2022.
  6. A. Naveed, H. J. Yang, J. Yang, Y. N. Nuli, and J. L. Wang, "Highly reversible and rechargeable safe Zn batteries based on a triethyl phosphate electrolyte," *Angewandte Chemie International Edition*, vol. 58, pp. 2760-2764, 2019.
  7. P. Hei, Y. Sai, C. Liu, W. J. Li, J. Wang, X. Q. Sun, Y. Song, and X. X. Liu, "Facilitating the electrochemical oxidation of ZnS through iodide catalysis for aqueous zinc-sulfur batteries," *Angewandte Chemie International Edition*, vol. 136, no. 9, 2024.
  8. J. Zhi, S. K. Li, M. Han and P. Chen, "Biomolecule-guided cation regulation for dendrite-free metal anodes," *Science Advances*, vol. 6, no. 32, 2020.
  9. N. N. Zhang, S. Huang, Z. S. Yuan, J. C. Zhu, Z. F. Zhao and Z. Q. Niu, "Direct self-assembly of MXene on Zn anodes for dendrite-free aqueous zinc-ion batteries," *Angewandte Chemie International Edition*, vol. 60, pp. 2861-2865, 2021.
  10. L. T. Kang, M. W. Cui, F. Y. Jiang, Y. F. Gao, H. J. Luo, J. J. Liu, W. Liang, and C. Y. Zhi, "Nanoporous CaCO<sub>3</sub> coatings enabled uniform Zn stripping/plating for long-life zinc rechargeable aqueous batteries," *Advanced Energy Materials*, vol. 8, pp., 2018.
  11. W. T. Yuan, X. Y. Nie, Y. Y. Wang, X. T. Li, G. Q. Ma, Y. Wang, S. G. Shen, and N. Zhang, "Orientational electrodeposition of highly (002)-textured zinc metal anodes enabled by iodide ions for stable aqueous zinc batteries," *Acs Nano*, vol. 17, pp. 23861-23871, 2023.
  12. G. N. Qian, G. B. Zan, J. Z. Li, S. J. Lee, Y. Wang, Y. Y. Zhu, S. Gul, D. J. Vine, S. Lewis, W. B. Yun, Z. F. Ma, P. Pianetta, J. S. Lee, L. S. Li, and Y. J. Liu, "Structural, dynamic, and chemical complexities in zinc anode of an operating aqueous Zn-ion battery," *Advanced Energy Materials*, vol. 12, pp., 2022.
  13. Q. Zhao, S. Stalin, and L. A. Archer, "Stabilizing metal battery anodes through the design of solid electrolyte interphases," *Joule*, vol. 5, pp. 1119-1142, 2021.
  14. J. N. Hao, B. Li, X. L. Li, X. H. Zeng, S. L. Zhang, F. H. Yang, S. L. Liu, D. Li, C. Wu, and Z. P. Guo, "An in-depth study of zn metal surface chemistry for advanced aqueous Zn-ion batteries," *Advanced Materials*, vol. 32, pp., 2020.
  15. Y. J. Wang, N. Li, H. Y. Liu, J. Shi, Y. Q. Li, X. K. Wu, Z. Wang, C. Huang, K. Y. Chen, D. B. Zhang, T. Y. Wu, P. Li, C. X. Liu, and L. W. Mi, ""Zincophilic-hydrophobic" PAN/PMMA nanofiber membrane toward high-rate dendrite-free Zn anode," *Advanced Fiber Materials*, vol. 5, pp. 2002-2015, 2023.
  16. M. H. Zhang, J. H. Li, Y. W. Tang, D. W. Wang, H. S. Hu, M. T. Liu, B. Xiao, and P. F. Wang, "Selective Zn-ion channels enabled by a double-network protective layer for stable zinc anode," *Energy Storage Materials*, vol. 65, pp., 2024.
  17. M. Kwon, J. Lee, S. Ko, G. Lim, S. H. Yu, J. Hong, and M. Lee, "Stimulating Cu-Zn alloying for compact Zn metal growth towards high energy aqueous batteries and hybrid supercapacitors," *Energy & Environmental Science*, vol. 15, pp. 2889-2899, 2022.
  18. D. Yang, X. Y. Wu, L. He, H. N. Zhao, Y. Z. Wang, Z. Y. Zhang, J. Y. Qiu, X. B. Chen, and Y. J. Wei, "Ionic layer epitaxy growth of organic/inorganic composite protective layers for large-area Li and Zn metal anodes," *Nano Letters*, vol. 23, pp. 11152-11160, 2023.
  19. Y. Z. Wang, X. M. Xu, J. Yin, G. Huang, T. C. Guo, Z. N. Tian, R. Alsaadi, Y. P. Zhu, and H. N. Alshareef, "MoS<sub>2</sub>-mediated epitaxial plating of Zn metal anodes," *Advanced Materials*, vol. 35, no. 6, 2022.
  20. H. Wang, Q. Y. Li, S. Z. Huang, L. J. Zhou, L. Mei, Z. B. Wu, B. H. Qu, W. F. Wei, X. B. Ji, Y. J. Chen, and L. B. Chen, "Controlled deposition via a bifunctional layer enables dendrite-free zinc metal batteries," *Chemical Engineering Journal*, vol. 470, no. 15, p. 144147, 2023.
  21. Y. Tian, Y. L. An, C. L. Wei, B. J. Xi, S. L. L. Xiong, J. K. Feng, and Y. T. Qian, "Flexible and free-standing Ti<sub>3</sub>C<sub>2</sub>Tx MXene@Zn paper for dendrite-free aqueous zinc metal batteries and nonaqueous lithium metal batteries," *ACS Nano*, vol. 13, pp. 11676-11685, 2019.
  22. Z. Li, Z. Gong, X. Y. Wu, K. Ye, J. Yan, G. L. Wang, Y. J. Wei, K. Zhu, J. Yi, D. A. X. Cao, and G. H. Chen, "Dendrite-free and anti-corrosion Zn metal anode enabled by an artificial layer for high-performance Zn ion capacitor," *Chinese Chemical Letters*, vol. 33, pp. 3936-3940, 2022.
  23. Y. B. Mu, Z. Li, B. K. Wu, H. D. Huang, F. H. Wu, Y. Q. Chu, L. F. Zou, M. Yang, J. F. He, L. Ye, M. S. Han, T. S. Zhao, and L. Zeng, "3D hierarchical graphene matrices enable stable Zn anodes for aqueous Zn batteries," *Nature Communications*, vol. 14, pp., 2023.
  24. Q. Liu, R. L. Wang, Z. F. Liu, X. S. Wang, C. P. Han, H. B. Liu, and B. H. Li, "A 3D lithiophilic ZIF-8@RGO free-standing scaffold with dendrite-free behavior enabling high-performance Li metal batteries," *Journal of Materials Chemistry A*, vol. 11, pp. 12910-12917, 2023.
  25. Y. Yang, C. Y. Liu, Z. H. Lv, H. Yang, Y. F. Zhang, M. H. Ye, L. B. Chen, J. B. Zhao, and C. C. Li, "Synergistic manipulation of Zn<sup>2+</sup> ion flux and desolvation effect enabled by anodic growth of a 3D ZnF<sub>2</sub> matrix for long-lifespan and dendrite-free zn metal anodes," *Advanced Materials*, vol. 33, no. 11, 2021.
  26. C. Ogata, R. Kurogi, K. Hatakeyama, T. Taniguchi, M. Koinuma, and Y. Matsumoto, "All-graphene oxide device with tunable supercapacitor and battery behaviour by the working voltage," *Chemical Communications*, vol. 52, pp. 3919-3922, 2016.
  27. K. Y. Kwon, T. H. Jo, J. S. Kim, F. Hasan, and H. D. Yoo, "A chronocoulometric method to measure the corrosion rate on zinc metal electrodes," *ACS Applied Materials & Interfaces*, vol. 12, pp. 42612-42621, 2020.